Structural and Optical Properties of Mixed Diindenoperylene–Perfluoropentacene Thin Films

J. P. Reinhardt,[†] A. Hinderhofer,*[†,‡] K. Broch,[†] U. Heinemeyer,[†] S. Kowarik,[§] A. Vorobiev,[⊥] A. Gerlach,[†] and F. Schreiber*[†]

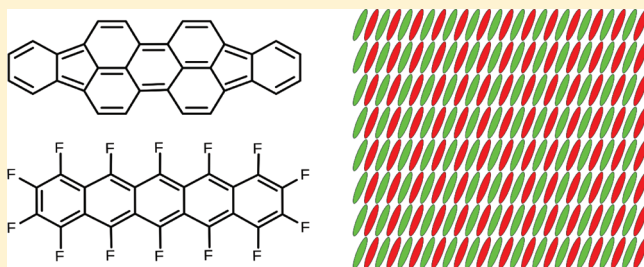[†]Institute for Applied Physics, University of Tübingen, Tübingen, Germany
[‡]Graduate School of Advanced Integration Science, Chiba University, Chiba, Japan
[§]Institute for Physics, Humboldt University Berlin, Berlin, Germany
[⊥]European Synchrotron Radiation Facility (ESRF), Grenoble, France

S *Supporting Information*

ABSTRACT: Mixed films of perfluorinated pentacene and diindenoperylene are studied for their structural and optical properties on SiO_2 and glass substrates. Grazing incidence X-ray diffraction shows that the compounds mix on the molecular level. Two structures are identified. Their out-of-plane lattice spacing is determined by X-ray reflectivity, and their growth morphology is characterized using atomic force microscopy. It is found that one structure consists of molecules in a standing-up and the other in a lying-down orientation. The uniaxial dielectric function of mixed films is determined with spectroscopic ellipsometry, and the in-plane optical extinction coefficient is measured by real-time differential reflectance spectroscopy during growth. The question of intermolecular coupling between perfluorinated pentacene and diindenoperylene is discussed.

INTRODUCTION

Binary mixtures of organic materials in thin films have attracted significant attention, inter alia because of their extensive use as donor–acceptor bulk heterojunctions in organic photovoltaic devices[1,2] or as highly doped conductive layers in organic electronics.[3−6] A key question for the optical and structural properties of a mixture of two organic compounds is whether the materials are phase-separating or -mixing on the molecular level. Complete or partial mixing of two species may be possible if a mixed crystal exists that is energetically more favorable than two pure crystals. Of importance in this regard is the isostructural compatibility of both compounds, which is in many cases a prerequisite for efficient mixing.[7−10]

An ordered molecular mixture (molecular complex) may be formed due to strong interaction between certain parts of the mixed compounds. In this context, by molecular complex we mean an ordered, mixed crystal that is built up by sufficiently strong interaction (e.g. electrostatic or hydrogen bond), which does not necessarily involve a significant charge transfer in the ground state between the compounds involved. One such interaction forming molecular complexes is, for example, the arene/perfluoroarene interaction.[11−13] In single crystals, the interaction between arenes and perfluorinated arenes leads to pronounced face-to-face stacking, which was also described as dimerization in the crystal.[14] Therefore, these complexes exhibit a simple molar mixing ratio, mostly 1:1[11,15−17] or 2:1.[18] In contrast to bulk single crystal growth, in which the

minimization of lattice energy is the most relevant driving force, structure formation of thin films is often far from thermal equilibrium. For the full description of thin film structure formation, one also has to account for kinetic growth effects.[19,20] The mixing behavior in such multicomponent organic thin films is as yet not well understood, and in fact, even the growth and structure of single-component thin films are already nontrivial.[21,22]

Recently, the formation of an equimolar molecular complex of pentacene (PEN) and perfluoropentacene (PFP)[23−30] upon coevaporation were reported in thin films,[9,25] which exhibits interesting optical and electrical characteristics.[17,31−33] The formation of this molecular complex of PEN and PFP is also facilitated by the steric compatibility of both compounds.

The present paper is dedicated to a detailed analysis of the optical and structural characteristics of PFP/DIP mixed thin films. Diindenoperylene (DIP)[34−37] is a promising candidate for use in organic photovoltaics (OPV) because of its high structural order[20,38] and its ability to function as an efficient electron donor[39] for OPV applications. The combination of PFP and DIP might be of potential interest for photovoltaics, since it would absorb light in a wide frequency range, and the electronic energy levels might enable efficient exciton diffusion.

For PFP/DIP, the sterical compatibility of both species is lower compared with the combination of PFP/PEN, since DIP has a different shape and is larger than PFP (Figure 1).
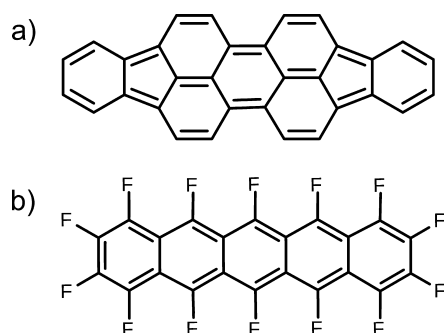

Figure 1. Molecular structure of (a) diindenoperylene (DIP) and (b) perfluorinated pentacene (PFP).

Therefore, the question arises whether the expected arene/perfluoroarene interaction is strong enough to enable complex formation also for these sterically less compatible compounds. The present paper addresses this question using X-ray diffraction, atomic force microscopy, and optical spectroscopy. Note that growth and structure of DIP/PFP *planar* multilayer heterostructures without mixing were studied in refs 40 and 41.

■ EXPERIMENTAL SECTION

Mixed thin films with three different mixing ratios (1:1, 1:3, 3:1) of PFP and DIP were coevaporated by organic molecular beam deposition.[21,22,42] The estimated error of the mixing ratios is ±10%. The materials (Figure 1) PFP (Kanto Denka Kogyo Co., Japan, with 99% purity) and DIP (Institut für PAH Forschung Greifenberg, Germany, with 99.9% purity) were obtained commercially. DIP was purified by gradient sublimation before use. PFP was used as received.

The thin films were prepared at a base pressure of 2×10^{-10} mbar on three different substrates: silicon wafers with a native oxide layer of ∼1.5 nm thickness, a thermal oxide layer of ∼147 nm, and 0.5 mm-thick glass substrates. All substrates were cut into slices of ∼0.5 cm² and cleaned in an ultrasonic bath subsequently with acetone, isopropyl alcohol, and ultrapure water for 5 min each. The growth rate was 1 Å/min for each compound, controlled with a water-cooled quartz crystal microbalance calibrated by X-ray reflectivity. Films were grown at three different growth temperatures, T (300, 330, and 360 K), and with thicknesses of 10, 20, and 30 nm.

The film thicknesses, roughness and interlayer lattice spacings were determined from X-ray reflectivity (XRR)[43] using Cu K$_{\alpha 1}$ radiation ($\lambda = 1.5406$ Å). Fitting of XRR data was performed with MOTOFIT[44] using the Parratt formalism. The in-plane crystal structure was measured with grazing incidence X-ray diffraction (GIXD)[43] at the ID10B beamline of the European Synchrotron Radiation Facility (ESRF), $\lambda = 0.925$ Å. For GIXD, an angle of incidence of $\alpha_i = 0.11°$ was used. The morphology of the thin films was characterized using atomic force microscopy (AFM) in oscillating noncontact mode (JPK NanoWizard II).

The uniaxial anisotropic optical constants were determined by a multisample analysis from variable angle spectroscopic ellipsometry (VASE) data as described in refs 26, 45, and 46. Real-time measurements of the in-plane extinction coefficient were made using differential reflectance spectroscopy

(DRS)[47,48] for monitoring changes during growth. The DRS setup uses a halogen light source and a CCD-array spectrometer (Ocean Optics). The detection range with good signal was between 1.5 and 2.8 eV. The DRS signal is calculated from the reflectivity of the bare substrate $R(0)$ and the reflectivity $R(d)$ at thickness d:

$$\Delta_{DRS} = \frac{R(d) - R(0)}{R(0)} \tag{1}$$

Δ_{DRS} describes the relative change in reflectivity, which is a first approximation for very thin films proportional to the imaginary part of the dielectric function of the film.[49] DRS data were analyzed numerically as described in ref 45 using the full formalism that is applicable also for thicker films.

■ RESULTS

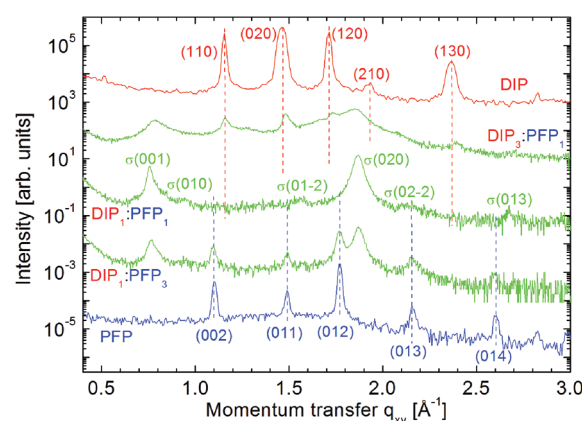**GIXD of DIP/PFP Thin Films.** Figure 2 shows GIXD data of DIP/PFP mixed films with three different mixing ratios

Figure 2. GIXD of DIP/PFP mixed films with three different mixing ratios (DIP$_1$/PFP$_1$, DIP$_3$/PFP$_1$, DIP$_1$/PFP$_3$) compared with GIXD data from the pure films. All films were grown at $T = 330$ K on SiO$_2$ with a nominal thickness of $d = 20$ nm. Data from each scan were normalized on the maximum peak value and shifted in absolute intensity for clarity. The pure films data were indexed after crystal structures from the literature.[23,25,50] The 1:1 mixture is indexed after the unit cell described in Table 2.

(DIP$_1$/PFP$_1$, DIP$_3$/PFP$_1$, DIP$_1$/PFP$_3$) compared with GIXD data from the pure films. All films were grown at $T = 330$ K on SiO$_2$ with a nominal thickness of $d = 20$ nm. The pure DIP film exhibits only reflections from the DIP hig-temperature phase (HT phase, P21/a polymorph),[50] which is commonly observed in thin films of DIP.[20,38,51] The pure PFP film exhibits only reflections from the PFP thin film phase.[23−25] Note that PFP thin films grow textured with the *bc* plane parallel to the substrate. The DIP crystallites are oriented with the *ab* plane parallel to the substrate. Both orientations correspond roughly to a standing-up configuration of molecules relative to the substrate.

The DIP$_1$/PFP$_1$ film exhibits six in-plane reflections marked σ(*hkl*). For indexing, the tentative in-plane unit cell from Table 2 is used. Peak positions of the molecularly mixed DIP$_1$/PFP$_1$ film were fitted with Lorentzian functions and a linear background (Table 1). The positions of these in-plane reflections do not coincide with the peak positions of the pure materials. From this observation, we conclude that coevaporated DIP/PFP films are mixed on the molecular

Table 1. Fitted Bragg Peak Positions of the DIP$_1$/PFP$_1$ Mixed Film

peak	$\sigma(h01)$	$\sigma(h10)$	$\sigma(h1\text{-}2)$	$\sigma(h20)$	$\sigma(h2\text{-}2)$	$\sigma(h13)$
q_{xy} (Å^{-1})	0.77	0.91	1.57	1.86	2.15	2.67

level and form a common crystal structure. The DIP$_3$/PFP$_1$ and DIP$_1$/PFP$_3$ mixed films exhibit in-plane reflections from the pure DIP or PFP thin film structures, respectively, depending on the volume fractions of each compound. In addition, in these mixed films, we find reflections of the mixed structure at the same q_{xy} positions as in the 1:1 mixed film, indicating that the unit cell of the mixed structure does not depend strongly on the mixing ratio. This coexistence of both the pristine film structures and the 1:1 mixed film structure is an indication that the structure of DIP/PFP mixed films does not change continuously with the mixing ratio. We conclude that DIP and PFP form an equimolar molecular complex upon coevaporation similar to the PEN/PFP mixed films studied in ref 9. Excess molecules of either species are phase-separating in their respective pure film structure.

Tentative Lattice Parameters for DIP/PFP Mixed Films. Figure 3 shows a reciprocal space map from a DIP$_1$/
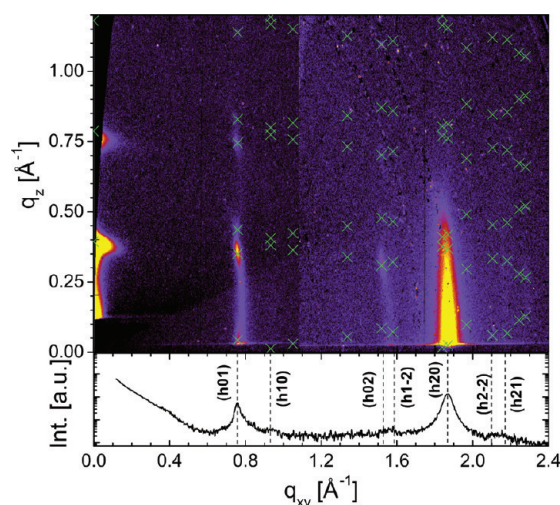

Figure 3. Reciprocal space map (RSM) from a 20 nm DIP$_1$/PFP$_1$ film measured with a CCD area detector. At the bottom, GIXD data measured with a point detector at an angle incidence of $\alpha_i = 0.11°$ are shown for comparison. The film was grown at $T = 330$ K on SiO$_2$ with a nominal thickness of $d = 20$ nm. The RSM was assembled from two CCD images with different count rates, which results in different noise levels on the right and left sides of the image. Crosses indicate theoretical positions of reflections for the proposed unit cell.

PFP$_1$ mixed film recorded with a CCD area detector. At the bottom, GIXD data measured with a point detector are shown for comparison and with the indexing of the proposed unit cell. Crosses in Figure 3 mark theoretical peak positions of the proposed unit cell for the DIP$_1$/PFP$_1$ molecular complex. For

calculation of theoretical peak positions, we assumed that the DIP$_1$/PFP$_1$ film is fiber-textured; that is, grains are oriented with their bc plane parallel to the substrate and have azimuthally a random orientation. The parameters of the proposed unit cell, which probably contains one molecule of each species, are shown in Table 2. For these parameters, the unit cell volume of the mixture lies between the pure crystals unit cell volumes. We note again that PFP and DIP/PFP thin films usually grow textured, oriented with the bc plane parallel to the substrate. The DIP crystallites are oriented with the ab plane parallel to the substrate. Both orientations correspond roughly to a standing-up configuration of molecules within the respective unit cells.

We note also that both PFP and DIP have an in-plane unit cell angle of $\gamma = 90°$ for DIP and $\alpha = 90°$ for PFP; however, in 1:1 arene/perfluoroarene complexes with compounds that are structurally different, the unit cell may exhibit only low symmetry,[16] that is, the in-plane unit cell deviates significantly from 90°.

Molecular Orientation in DIP/PFP Complexes. In Figure 4a, XRR data of DIP$_1$/PFP$_1$ mixed films with different
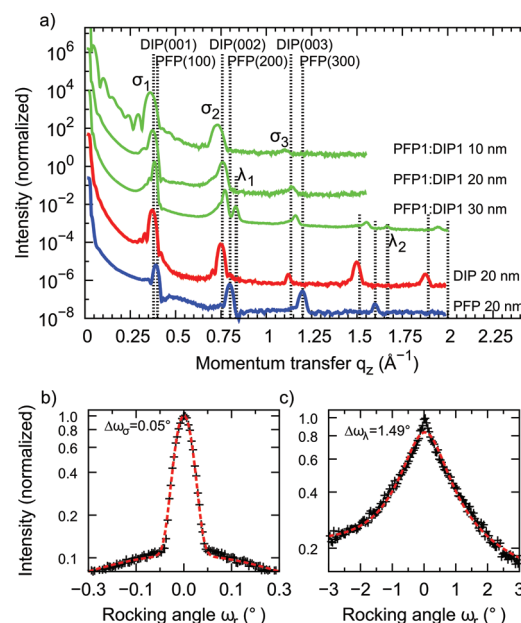

Figure 4. (a) XRR data of DIP$_1$/PFP$_1$ mixed films grown at 330 K together with two scans from the respective pure films. The XRR data were shifted on the intensity axis for clarity. (b) Rocking scan performed on the σ_2 reflection. (c) Rocking scan on the λ_1-reflection. Both rocking scans were normalized on the maximum peak value. The dashed lines show the fits used to extract the mosaicity.

thicknesses are shown and compared with XRR data from pure DIP and PFP films. At least two orientations are present in DIP$_1$/PFP$_1$ mixtures. All mixed films exhibit at least a first- and second-order Bragg reflection corresponding to nearly standing

Table 2. Proposed Lattice Parameters of DIP/PFP Mixtures and Parameters of Pure DIP and PFP

	a (nm)	b (nm)	c (nm)	α (deg)	β (deg)	γ (deg)	V_{cell} (nm^3)
PFP[25]	1.576	0.451	1.148	90.0	90.4	90.0	0.816
DIP$_1$/PFP$_1$	1.6(0)	0.69(3)	0.85(3)	104.(0)	93.(1)	~90	0.917
DIP[50]	0.717	0.855	1.680	90.0	92.41	90.0	1.029

10919

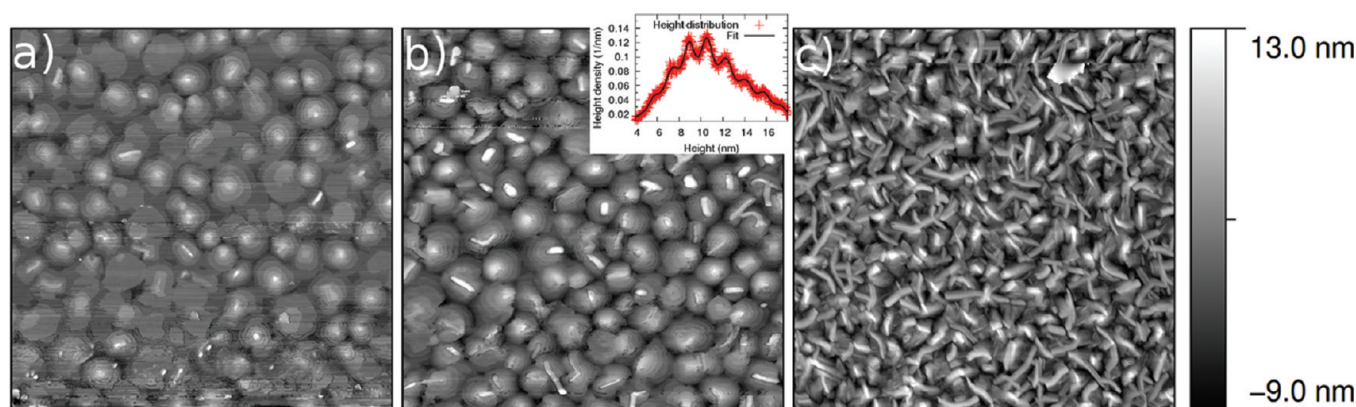dx.doi.org/10.1021/jp211947y | J. Phys. Chem. C 2012, 116, 10917−10923

Figure 5. AFM images of DIP_1/PFP_1 mixed films at three different thicknesses. The image size is 5×5 μm^2. All films were grown at 330 K with thicknesses of (a) 10, (b) 20, and (c) 30 nm. The inset in part b shows the height distribution of a 20 nm sample.

molecules (σ orientation). Using the indexing from Table 2, these peaks are the (100) and (200) reflections.

The out-of-plane lattice spacing is $d_\perp \sim 1.62$ nm, as determined from the 30 nm film shown in Figure 4a. The lattice spacing lies between the lattice spacings of DIP ($d_\perp = 1.66$ nm) and PFP ($d_\perp = 1.57$ nm). The mixture with $d = 30$ nm exhibits, in addition, a Bragg reflection at $q_z = 0.836$ Å^{-1}, corresponding to a lattice spacing of $d_\perp = 0.75$ nm. This peak corresponds to the $(10{-}1)$ reflection using the indexing from Table 2 and is likely to originate from approximately lying-down molecules (λ orientation).

Rocking scans performed on the (200) Bragg reflection (σ orientation) and from the (10-1) reflection (λ orientation) are shown in Figure 4b,c to compare the mosaicity of the differently oriented domains. Both rocking scans were fitted with Lorentzian functions. The rocking scan on the reflection of the σ orientation consists of a sharp peak (fwhm = 0.05 ± 0.01°) and a broad background. In the rocking scan from the Bragg reflection related to the λ orientation, the intensity of both the diffuse scattering and the Bragg scattering are superimposed with a similar fwhm, ~1.5 ± 0.2°. We conclude that the mosaicity of the λ structure is significantly larger than the mosaicity of the σ structure.

The relative intensity of the λ_1 Bragg reflection is increased in thick films compared with thin films. The nucleation of λ-orientated domains may therefore be thickness-dependent, similar to the λ structure formation in pure DIP.[42] The nucleation of differently oriented domains depends also on growth temperature: high growth temperatures (90 °C) induce more-pronounced σ structure peaks and less-pronounced λ structure peaks (see the Supporting Information).

We note here that the mixed film formation of DIP/PFP is similar to PEN/PFP mixtures studied in ref 9. Both mixed films form a molecular complex with equimolar content. In addition, both thin film mixtures exhibit a σ structure with nearly upright-standing molecules and low mosaicity and a λ structure with the long molecular axis parallel to the substrate and large mosaicity. Compared with PEN/PFP mixtures, the out-of-plane lattice spacings of both DIP/PFP structures are slightly increased due to the larger DIP molecule.

Step Height and Thin Film Morphology from AFM. The two different orientations found with XRR are also observed in AFM measurements. AFM images corresponding to the XRR data thickness series (Figure 4a) are shown in Figure 5. Mainly growth of approximately circular islands is observed. The island diameters depend on growth temperature

and are largest for 330 K. The circular islands are identified as the σ orientation, which is done by comparing the step height measured for circular island growth to the interlayer lattice spacing calculated from the σ reflection peaks in X-ray reflectivity.

A typical height distribution of a mixed thin film ($d = 20$ nm) grown at 330 K is shown as an inset in Figure 5b. The height distribution shows eight different terraces. The step height was retrieved by fitting Gaussians to the height distribution and calculating the distances between the Gaussian centers. The final step height (1.63 ± 0.09 nm) was averaged over the calculated step heights from multiple AFM images. This step height retrieved from AFM is consistent with the step height of the σ structure retrieved from XRR.

A different growth morphology appears for thicker films, as shown in Figure 5c. The emergence of the new growth morphology correlates with the emergence of λ-structure peaks in the XRR data and is therefore thought to be due to the lying structure.

Optical Properties of DIP/PFP. For the discussion of the optical data, we focus on 1:1 mixtures, since only films with this mixing ratio form a completely mixed structure, whereas 3:1 and 1:3 films exhibit significant phase coexistence.

According to the polycrystalline film structure of the mixture, uniaxial optical anisotropy is found where the in-plane component of the dielectric function (i.e. relative to the substrate) differs from the out-of-plane component. Figure 6 shows the in-plane κ_{xy} and out-of-plane κ_z extinction coefficients of PFP, DIP, and DIP_1/PFP_1 films measured with VASE on SiO$_2$. These data are consistent with κ_{xy} measured with DRS on glass. Note that in Figure 6, κ_{xy} and κ_z of PFP and DIP were multiplied by 0.5. Vertical broken lines depict the absorption bands of the pure materials marked with the respective transition. For example, $S_{00}{-}S_{10}$ marks the transition between the singlet ground state S_{00} and the first excited state S_{10}. Vibronic excitations are denoted with S_{1i}. "DIP*" marks another transition of DIP, which does not belong to the vibronic progression.[37,48] For further details and, in particular, the theoretical background of vibrational excitations in DIP, see ref 52.

To check whether significant intermolecular electronic coupling between both compounds is present, we simulated the anisotropic extinction coefficient of the mixture with effective medium approximations (EMA) based on data of the pure materials.[26,37] EMA models cannot describe effects from microscopic intermolecular coupling. Therefore, if the optical
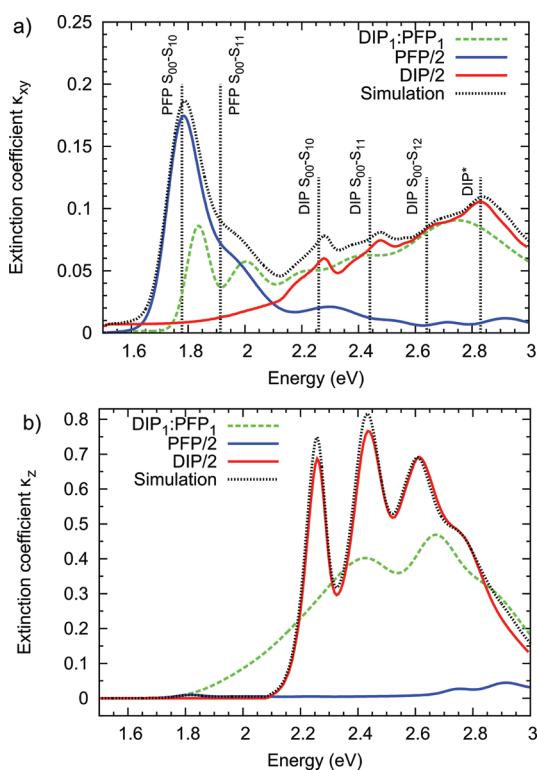
10920

dx.doi.org/10.1021/jp211947y | J. Phys. Chem. C 2012, 116, 10917–10923

Figure 6. In-plane extinction coefficients κ_{xy} (a) and out-of-plane extinction coefficients κ_z (b) of PFP, DIP, and DIP/PFP thin films ($d \sim 20$ nm) measured with VASE on SiO$_2$. Extinction coefficients of the pure films originate from refs 26 and 37. κ from pure PFP and DIP were divided by 2. The vertical lines depict the transition energies in the pure films. Simulations of κ_{xy} and κ_z of the mixtures were calculated using the Maxwell−Garnett EMA[53] with data from pure samples.

properties of the mixture can be modeled sufficiently well by an effective medium approximation, contributions from intermolecular coupling on κ would be insignificant in the mixture.

We employed three different EMA models to simulate the DIP$_1$/PFP$_1$ mixture: a linear superposition of extinction coefficients ($\kappa_{PFP}/2 + \kappa_{DIP}/2$) and the Bruggeman[54] and the Maxwell−Garnett[53] methods. None of these models describes κ_{xy} and κ_z of the mixture correctly. The Maxwell−Garnett simulation, which showed a maximum of overlap with the experimental data, is shown for comparison in Figure 6. The significant differences between the simulation and the experimentally determined extinction coefficients are a hint for a change in intermolecular electronic coupling in the DIP$_1$/PFP$_1$ mixture compared with the pure films; however, new, pronounced, and clearly discernible transitions are not observed in the measured energy range. This is in contrast to molecular complexes of PEN$_1$/PFP$_1$, in which a new transition presumably related to an excited charge transfer state is observed.[17]

In the following, we analyze the differences between the simulated and the experimental optical spectra in more detail. Since the fitted out-of-plane extinction coefficient of a uniaxial thin film is very sensitive to small uncertainties in the applied model,[46,55] we focus on the analysis of the more reliable in-plane component.

First, a feature not explained by the EMA simulation is the change of oscillator strengths of the first absorption band of PFP (S$_{00}$−S$_{10}$) in the mixture. Whether the redistribution of oscillator strengths in the mixture compared with the

simulation is induced through "coupling" of the different species (DIP−PFP interaction) or "isolation" (reduced PFP−PFP and DIP−DIP interaction) is not obvious. Second, we observe a difference in energy positions in the mixture compared with the simulation. In Table 3, we list the peak

Table 3. Energy Positions of the Absorption Bands in Pure PFP, DIP, and DIP$_1$/PFP$_1$ Mixed Films

peak	energy positions (eV)		
	PFP[17]	DIP$_1$/PFP$_1$	DIP[37]
PFP S$_{00}$−S$_{10}$	1.75	1.83	
PFP S$_{00}$−S$_{11}$	1.94	2.00	
DIP S$_{00}$−S$_{10}$		2.18	2.25
DIP S$_{00}$−S$_{11}$		2.38	2.48
DIP S$_{00}$−S$_{12}$		2.70	2.6
DIP*			2.8

positions of the pure materials with that of the mixture. Energy positions of the pure samples were determined in refs 17 and 37. The two peaks at lowest energy (1.83 and 2.00 eV) were assigned to correspond to the PFP S$_{00}$−S$_{10}$ and PFP S$_{00}$−S$_{11}$ transition. The assignment of the remaining peak maxima is not unambiguously possibly, since transitions of the pure PFP and DIP film spectra overlap in the energy region of 2.1−3.0 eV. Tentatively, we assign the observed three peak maxima to DIP transitions, which fit reasonably well in energy position and oscillator strength.

One obvious difference between the pure materials and the mixture is the blue shift of the first two transitions related to PFP in the experiment (1.83 eV) compared to the simulation (1.75 eV). Furthermore, the DIP* transition is significantly weaker in the experimental data compared with the simulation. This transition is associated with higher-order Frenkel and charge transfer excitations and closely coupled to the structural order in bulk DIP.[48] The weak intensity of this mode can therefore be interpreted by "isolation" of the DIP molecules due to the mixed in PFP molecules. The decrease of intensity in the DIP* transition results in an apparent blue shift of the superimposed DIP S$_{00}$−S$_{12}$ transition. In contrast, the DIP S$_{00}$−S$_{10}$ and DIP S$_{00}$−S$_{11}$ transitions experience an apparent red shift in the mixture and are more smeared out in comparison with the simulated spectrum. Several mechanisms may be responsible for the observed peak shifts.

A shift of the complete spectrum may be observed if the polarizability of a molecule's environment is changed (solvent shift). In the case of PFP/DIP mixtures, the refractive index (see the Supporting Information) is higher than that of pure PFP[26] and lower than that of pure DIP[37] for both components. This would imply a shift to lower energies for transitions related to PFP and to higher energies for transitions related to DIP. Since we observe the opposite behavior in the mixture (blue shift for PFP transitions, red shift for DIP transitions), the peak shifts cannot be explained by a simple solvent shift.

Another possible mechanism leading to a thickness dependent absorption peak shift is attributed to a dielectric screening effect due to a different volume-to-surface ratio for different thicknesses. This was observed for PFP[48] and also for growth of PTCDA,[56] but not for pure DIP growth at elevated temperatures.[48] To study the origin of the blue shift of the PFP absorption band in the mixture in more detail, real-time measurements on a DIP$_1$/PFP$_1$ mixture on a glass substrate were performed using DRS. A comparison of κ_{xy} from real-time

DRS and from a simulation of a DIP_1/PFP_1 mixture for different thicknesses is shown in Figure 7a. For simulating the thickness-dependent κ_{xy}, again, the Maxwell−Garnett method is employed using experimental real-time data of the pure materials on glass.
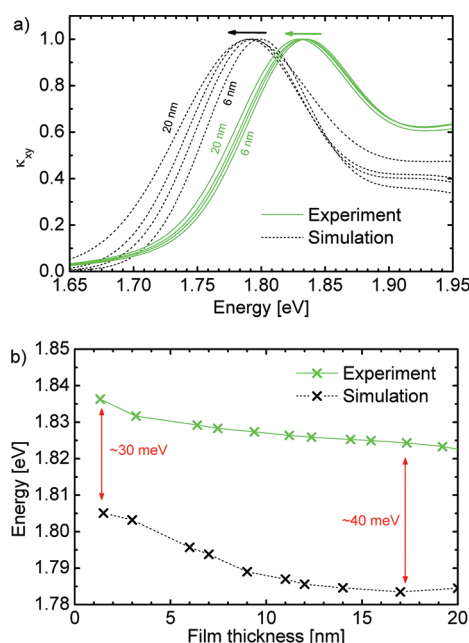

Figure 7. (a) Comparison of the normalized in-plane extinction coefficients κ_{xy} from real-time DRS and from a simulation of a DIP_1/PFP_1 mixture. DRS data were measured during film growth on a glass substrate. The simulated κ_{xy} were calculated from the real-time evolution of the pure materials on glass with a Maxwell−Garnett EMA model. (b) Peak position of the HOMO−LUMO transition from the simulation and the experimental data from DIP_1/PFP_1.

The thickness-dependent energy positions of the first transitions are shown in Figure 7b for both data sets. Simulated κ_{xy} values exhibit the typical red shift of the first absorption band versus film thickness ($\sim$20 meV)[48] associated with the PFP $S_{00}-S_{1i}$ transitions. In comparison with the simulated data, the red shift of the PFP $S_{00}-S_{10}$ transition versus film thickness in the DIP_1/PFP_1 experimental data is smaller ($\sim$10 meV). This discrepancy may be explained by a reduction of the dielectric screening effect by the mixed-in DIP molecules or a slightly different morphology in the mixed films; however, the absolute difference of the PFP $S_{00}-S_{1i}$ energy positions between the mixture and the simulation (30−40 meV) is found for each thickness. We conclude that the thickness-dependent screening effect as described in refs 48 and 56 is also observed for mixed PFP/DIP films; however, this effect seems to be not related to the observed blue shift of the PFP $S_{00}-S_{10}$ and $S_{00}-S_{11}$ transitions in the mixed films compared with pure PFP.

In general, arene/perfluoroarene complexes are formed by a combination of electrostatic quadrupole−quadrupole interaction and dispersion forces.[11,13] The influences of these microscopic intermolecular coupling effects between DIP and PFP on the absorption energy, including the reorganization energy, is not entirely understood for solid-state binary mixtures and may be the source of the observed peak shifts discussed above.

SUMMARY AND CONCLUSIONS

We have studied the structural and optical properties of mixed DIP/PFP thin films. Despite the size difference of the compounds, an equimolar ordered molecular complex forms upon codeposition with a unit cell containing both PFP and DIP molecules. The mixed thin films are composed of two differently oriented domains. The σ structure has an interlayer lattice spacing that indicates almost standing molecules. For films thicker than 20 nm, another structure (λ structure) of molecules in a lying-down or strongly tilted orientation is observed. From the step height of the islands in AFM measurements, we conclude that the σ structure follows circular island growth similar to DIP. The λ structure is assigned to the rodlike growth morphology emerging for the higher film thicknesses. The optical properties of the DIP_1/PFP_1 thin films were measured using DRS and VASE. The optical constants of the mixed films can, in general, not be explained by an EMA model of the optical constants of the pure films. One important finding is the shift of the PFP $S_{00}-S_{10}$ transition to lower energies in the mixture, which may be explained by intermolecular coupling between neighboring PFP and DIP molecules in the molecular complex.

ASSOCIATED CONTENT

$\mathbf{S}$ Supporting Information

GIXD and XRR data from PFP/DIP mixtures prepared at different growth temperatures; uniaxial refractive index of PFP/DIP mixtures. This material is available free of charge via the Internet at http://pubs.acs.org.

AUTHOR INFORMATION

Corresponding Author

*Phone: +49 7071 29 78663. Fax: +49 7071 29 5110. E-mails: alexander.hinderhofer@chiba-u.jp; frank.schreiber@uni-tuebingen.de.

Notes

The authors declare no competing financial interest.

ACKNOWLEDGMENTS

REFERENCES

(1) Opitz, A.; Wagner, J.; Brütting, W.; Salzmann, I.; Koch, N.; Manara, J.; Pflaum, J.; Hinderhofer, A.; Schreiber, F. *IEEE J. Sel. Top. Quant. Electron.* **2010**, *16*, 1707.

(2) Brabec, C., Dyakonov, V., Parisi, J., Sariciftci, N., Eds.; *Organic Photovoltaics*; Springer: Berlin, Heidelberg, 2003.

(3) Walzer, K.; Maennig, B.; Pfeiffer, M.; Leo, K. *Chem. Rev.* **2007**, *107*, 1233−1271.

(4) Chen, W.-B.; Xiang, H.-F.; Xu, Z.-X.; Yan, B.-P.; Roy, V. A. L.; Che, C.-M.; Lai, P.-T. *Appl. Phys. Lett.* **2007**, *91*, 191109.

(5) Gao, W.; Kahn, A. *Appl. Phys. Lett.* **2001**, *79*, 4040−4042.

(6) Gao, W.; Kahn, A. *Appl. Phys. Lett.* **2003**, *82*, 4815−4817.

(7) Kitaigorodsky, A. In *Mixed Crystals*; Cardona, M., Ed.; Springer: Berlin, Heidelberg, 1984.

(8) Vogel, J. O.; Salzmann, I.; Duhm, S.; Oehzelt, M.; Rabe, J. P.; Koch, N. *J. Mater. Chem.* **2010**, *20*, 4055−4066.

(9) Hinderhofer, A.; Frank, C.; Hosokai, T.; Resta, A.; Gerlach, A.; Schreiber, F. *J. Chem. Phys.* **2011**, *134*, 104702.

(10) Hinderhofer, A.; Schreiber, F. *ChemPhysChem* **2012**, *13*, 628−643.

(11) Meyer, E. A.; Castellano, R. K.; Diederich, F. *Angew. Chem., Int. Ed.* **2003**, *42*, 1210−1250.

(12) Coates, G. W.; Dunn, A. R.; Henling, L. M.; Ziller, J. W.; Lobkovsky, E. B.; Grubbs, R. H. *J. Am. Chem. Soc.* **1998**, *120*, 3641−3649.

(13) Reichenbacher, K.; Suss, H. I.; Hulliger, J. *Chem. Soc. Rev.* **2005**, *34*, 22−24.

(14) Bacchi, S.; Benaglia, M.; Cozzi, F.; Demartin, F.; Filippini, G.; Gavezzotti, A. *Chem.—Eur. J.* **2006**, *12*, 3538−3546.

(15) Williams, J. H.; Cockcroft, J. K.; Fitch, A. N. *Angew. Chem., Int. Ed.* **1992**, *31*, 1655−1657.

(16) Collings, J. C.; Roscoe, K. P.; Thomas, R. L.; Batsanov, A. S.; Stimson, L. M.; Howard, J. A. K.; Marder, T. B. *New J. Chem.* **2001**, *25*, 1410−1417.

(17) Broch, K.; Heinemeyer, U.; Hinderhofer, A.; Anger, F.; Scholz, R.; Gerlach, A.; Schreiber, F. *Phys. Rev. B* **2011**, *83*, 245307.

(18) Watt, S. W.; Dai, C.; Scott, A. J.; Burke, J. M.; Thomas, R. L.; Collings, J. C.; Viney, C.; Clegg, W.; Marder, T. B. *Angew. Chem., Int. Ed.* **2004**, *43*, 3061−3063.

(19) Krause, B.; Schreiber, F.; Dosch, H.; Pimpinelli, A.; Seeck, O. H. *Europhys. Lett.* **2004**, *65*, 372.

(20) Kowarik, S.; Gerlach, A.; Sellner, S.; Schreiber, F.; Cavalcanti, L.; Konovalov, O. *Phys. Rev. Lett.* **2006**, *96*, 125504.

(21) Witte, G.; Wöll, C. *J. Mater. Res.* **2004**, *19*, 1889−1916.

(22) Schreiber, F. *Phys. Status Solidi* **2004**, *201*, 1037.

(23) Sakamoto, Y.; Suzuki, T.; Kobayashi, M.; Gao, Y.; Fukai, Y.; Inoue, Y.; Sato, F.; Tokito, S. *J. Am. Chem. Soc.* **2004**, *126*, 8138−8140.

(24) Kowarik, S.; Gerlach, A.; Hinderhofer, A.; Milita, S.; Borgatti, F.; Zontone, F.; Suzuki, T.; Biscarini, F.; Schreiber, F. *Phys. Status Solidi - RRL* **2008**, *2*, 120−122.

(25) Salzmann, I.; Duhm, S.; Heimel, G.; Rabe, J. P.; Koch, N.; Oehzelt, M.; Sakamoto, Y.; Suzuki, T. *Langmuir* **2008**, *24*, 7294−7298.

(26) Hinderhofer, A.; Heinemeyer, U.; Gerlach, A.; Kowarik, S.; Jacobs, R. M. J.; Sakamoto, Y.; Suzuki, T.; Schreiber, F. *J. Chem. Phys.* **2007**, *127*, 194705.

(27) Koch, N.; Gerlach, A.; Duhm, S.; Glowatzki, H.; Heimel, G.; Vollmer, A.; Sakamoto, Y.; Suzuki, T.; Zegenhagen, J.; Rabe, J. P.; Schreiber, F. *J. Am. Chem. Soc.* **2008**, *130*, 7300.

(28) Duhm, S.; Hosoumi, S.; Salzmann, I.; Gerlach, A.; Oehzelt, M.; Wedl, B.; Lee, T.-L.; Schreiber, F.; Koch, N.; Ueno, N.; Kera, S. *Phys. Rev. B* **2010**, *81*, 045418.

(29) Breuer, T.; Witte, G. *Phys. Rev. B* **2011**, *83*, 155428.

(30) Götzen, J.; Schwalb, C. H.; Schmidt, C.; Mette, G.; Marks, M.; Höfer, U.; Witte, G. *Langmuir* **2011**, *27*, 993−999.

(31) Salzmann, I.; Duhm, S.; Heimel, G.; Oehzelt, M.; Kniprath, R.; Johnson, R. L.; Rabe, J. P.; Koch, N. *J. Am. Chem. Soc.* **2008**, *130*, 12870−12871.

(32) Anger, F.; Osso, J. O.; Heinemeyer, U.; Broch, K.; Scholz, R.; Gerlach, A.; Schreiber, F. *J. Chem. Phys.* **2012**, *136*, 054701.

(33) Kowarik, S.; Broch, K.; Hinderhofer, A.; Schwartzberg, A.; Osso, J. O.; Kilcoyne, D.; Schreiber, F.; Leone, S. R. *J. Phys. Chem. C* **2010**, *114*, 13061−13067.

(34) Dürr, A. C.; Schreiber, F.; Ritley, K. A.; Kruppa, V.; Krug, J.; Dosch, H.; Struth, B. *Phys. Rev. Lett.* **2003**, *90*, 016104.

(35) Zhang, D.; Heinemeyer, U.; Stanciu, C.; Sackrow, M.; Braun, K.; Hennemann, L. E.; Wang, X.; Scholz, R.; Schreiber, F.; Meixner, A. J. *Phys. Rev. Lett.* **2010**, *104*, 056601.

(36) Barrena, E.; de Oteyza, D. G.; Sellner, S.; Dosch, H.; Osso, J. O.; Struth, B. *Phys. Rev. Lett.* **2006**, *97*, 076102.

(37) Heinemeyer, U.; Scholz, R.; Gisslén, L.; Alonso, M. I.; Ossó, J. O.; Garriga, M.; Hinderhofer, A.; Kytka, M.; Kowarik, S.; Gerlach, A.; Schreiber, F. *Phys. Rev. B* **2008**, *78*, 085210.

(38) Dürr, A. C.; Schreiber, F.; Muench, M.; Karl, N.; Krause, B.; Kruppa, V.; Dosch, H. *Appl. Phys. Lett.* **2002**, *81*, 2276.

(39) Wagner, J.; Gruber, M.; Hinderhofer, A.; Wilke, A.; Bröker, B.; Frisch, J.; Amsalem, P.; Vollmer, A.; Opitz, A.; Koch, N.; Schreiber, F.; Brütting, W. *Adv. Funct. Mater.* **2010**, *20*, 4295.

(40) Hinderhofer, A.; Hosokai, T.; Frank, C.; Novák, J.; Gerlach, A.; Schreiber, F. *J. Phys. Chem. C* **2011**, *115*, 16155−16160.

(41) Hinderhofer, A.; Gerlach, A.; Kowarik, S.; Zontone, F.; Krug, J.; Schreiber, F. *Europhys. Lett.* **2010**, *91*, 56002.

(42) Kowarik, S.; Gerlach, A.; Schreiber, F. *J. Phys.: Condens. Matter* **2008**, *20*, 184005.

(43) Als-Nielsen, J.; McMorrow, D. *Elements of Modern X-ray Physics*; Wiley: New York, 2001.

(44) Nelson, A. *J. Appl. Crystallogr.* **2006**, *39*, 273−276.

(45) Heinemeyer, U. *Optical properties of organic semiconductor thin films: Static spectra and real-time growth studies*; Ph.D. thesis, Eberhard-Karls Universität, Tübingen, 2009.

(46) Bortchagovsky, E. *Thin Solid Films* **1997**, *307*, 192−199.

(47) Forker, R.; Fritz, T. *Phys. Chem. Chem. Phys.* **2009**, *11*, 2129.

(48) Heinemeyer, U.; Broch, K.; Hinderhofer, A.; Kytka, M.; Scholz, R.; Gerlach, A.; Schreiber, F. *Phys. Rev. Lett.* **2010**, *104*, 257401.

(49) McIntyre, J. D. E.; Aspnes, D. E. *Surf. Sci.* **1971**, *24*, 417−434.

(50) Heinrich, M. A.; Pflaum, J.; Tripathi, A. K.; Frey, W.; Steigerwald, M. L.; Siegrist, T. *J. Phys. Chem. C* **2007**, *111*, 18878.

(51) Kowarik, S.; Gerlach, A.; Sellner, S.; Cavalcanti, L.; Konovalov, O.; Schreiber, F. *Appl. Phys. A: Mater. Sci. Process.* **2009**, *95*, 233−239.

(52) Scholz, R.; Gisslen, L.; Schuster, B.-E.; Casu, M. B.; Chassé, T.; Heinemeyer, U.; Schreiber, F. *J. Chem. Phys.* **2011**, *134*, 014504.

(53) Wood, D. M.; Ashcroft, N. W. *Philos. Mag.* **1977**, *35*, 269.

(54) Bruggeman, D. A. G. *Ann. Phys.* **1935**, *24*, 686.

(55) Heinemeyer, U.; Hinderhofer, A.; Alonso, M. I.; Ossó, J. O.; Garriga, M.; Kytka, M.; Gerlach, A.; Schreiber, F. *Phys. Status Solidi A* **2008**, *205*, 927.

(56) Proehl, H.; Nitsche, R.; Dienel, T.; Leo, K.; Fritz, T. *Phys. Rev. B* **2005**, *71*, 165207.